IOP PUBLISHING PHYSICS IN MEDICINE AND BIOLOGY
Phys. Med. Biol. **57** (2012) 4555–4567 doi:10.1088/0031-9155/57/14/4555

Whole body sodium MRI at 3T using an asymmetric birdcage resonator and short echo time sequence: first images of a male volunteer

Friedrich Wetterling[1], Dominique M Corteville[1], Raffi Kalayciyan[1], Andreas Rennings[2], Simon Konstandin[1], Armin M Nagel[3], Helmut Stark[4] and Lothar R Schad[1]

[1] Computer Assisted Clinical Medicine, Heidelberg University, Mannheim, Germany
[2] General and Theoretical Electrical Engineering, University of Duisburg-Essen, 47057 Duisburg, Germany
[3] German Cancer Research Centre (DKFZ), Department of Medical Physics in Radiology, Heidelberg University, Heidelberg, Germany
[4] Stark Contrast GmbH, Erlangen, Germany

E-mail: wetterlf@tcd.ie

Received 2 October 2011, in final form 13 May 2012
Published 22 June 2012
Online at stacks.iop.org/PMB/57/4555

Abstract
Sodium magnetic resonance imaging (^{23}Na MRI) is a non-invasive technique which allows spatial resolution of the tissue sodium concentration (TSC) in the human body. TSC measurements could potentially serve to monitor early treatment success of chemotherapy on patients who suffer from whole body metastases. Yet, the acquisition of whole body sodium (^{23}Na) images has been hampered so far by the lack of large resonators and the extremely low signal-to-noise ratio (SNR) achieved with existing resonator systems. In this study, a ^{23}Na resonator was constructed for whole body ^{23}Na MRI at 3T comprising of a 16-leg, asymmetrical birdcage structure with 34 cm height, 47.5 cm width and 50 cm length. The resonator was driven in quadrature mode and could be used either as a transceiver resonator or, since active decoupling was included, as a transmit-only resonator in conjunction with a receive-only (RO) surface resonator. The relative B_1-field profile was simulated and measured on phantoms, and 3D whole body ^{23}Na MRI data of a healthy male volunteer were acquired in five segments with a nominal isotropic resolution of ($6 \times 6 \times 6$) mm^3 and a 10 min acquisition time per scan. The measured SNR values in the ^{23}Na-MR images varied from 9 ± 2 in calf muscle, 15 ± 2 in brain tissue, 23 ± 2 in the prostate and up to 42 ± 5 in the vertebral discs. Arms, legs, knees and hands could also be resolved with applied resonator and short time-to-echo (TE) (0.5 ms) radial sequence. Up to fivefold SNR improvement was achieved through combining the birdcage with local RO surface coil. In conclusion, ^{23}Na MRI of the entire human body provides

sub-cm spatial resolution, which allows resolution of all major human body parts with a scan time of less than 60 min.

S Online supplementary data available from stacks.iop.org/PMB/57/4555/mmedia

(Some figures may appear in colour only in the online journal)

1. Introduction

^{23}Na magnetic resonance imaging (^{23}Na MRI) is a non-invasive imaging technique, which enables the measurement of the tissue sodium concentration (TSC) in humans. The direct link of the TSC with the tissue integrity and viability (Thulborn *et al* 1999a, Ouwerkerk *et al* 2007) provides a promising approach for monitoring tumorous tissue elimination after chemotherapy (Schepkin *et al* 2005). However, ^{23}Na MRI is challenging because of the low *in vivo* abundance, the fast transversal relaxation rate and the low gyromagnetic ratio of the ^{23}Na ions in human tissue. Detectable ^{23}Na MRI signal generally originates from regions with high ^{23}Na content, such as extracellular fluids (i.e. blood, CSF and interstitial space) with an approximate ^{23}Na concentration of approximately 140 mM (Thulborn *et al* 1999b) , or cartilage, wherein negatively charged collagen attracts ^{23}Na ions into the spinal disc and knee joints resulting in high ^{23}Na concentration of ∼320 mM (Shapiro *et al* 2000).

Nearly all human body parts and organs have been examined separately with ^{23}Na MRI in earlier studies, including the head (Hilal *et al* 1985), the heart (Parish *et al* 1997), the kidneys (Maril *et al* 2006), the spine (Insko *et al* 2002) and the knees (Staroswiecki *et al* 2010). In order to cover multiple organs in one scan, dedicated resonator systems are required which provide sufficiently large field of view as well as sufficiently high receive sensitivity. While ^{1}H whole body resonators are commonly in-built in clinical MRI systems, the lack of whole body ^{23}Na-resonator for transmit-only (TO) purposes and the subsequent lack of B_1-field homogeneity for ^{23}Na MRI make it difficult to quantify the TSC with existing ^{23}Na techniques. In recent years, some groups have made use of the Helmholtz design in order to homogenize the ^{23}Na B_1-field for human ^{23}Na MRI (Steidle *et al* 2004, Ra *et al* 1988). Whole body resonators may offer an alternative to the Helmholtz design for X-nuclei MRI as has been demonstrated for ^{129}Xe- (Purea *et al* 2010) and ^{3}He-MRI of the human lungs at 1.5T (De Zanche *et al* 2008). More recently, coils with a highly homogeneous B_1-field enabled the exact measurement of subtle regional variations in local TSC via quantitative ^{23}Na MRI in a rodent stroke model (Wetterling *et al* 2010).

Besides the rf-resonator system, sequences designed to the special relaxation properties of the ^{23}Na ions are required, i.e. sequences with short TE (Boada *et al* 1997a, 1997b, 1997c, Jerecic *et al* 2004, Konstandin *et al* 2011, Nielles-Vallespin *et al* 2007). In non-liquids such as soft tissue and bone, 60% of the ^{23}Na-signal decays with short T_2^* (0.5–5 ms) and 40% decays with long T_2^* (20–50 ms) (Hilal *et al* 1985). Previously published ^{23}Na studies reporting on scans of multiple organs have suffered from long TE. For instance, spin echo sequence with radial k-space sampling and 14 ms TE was used to examine the heart, liver, gallbladder, spine and kidneys in three separate scans (Ra *et al* 1988). Only modest image quality was achieved. Later gradient echo sequence and Cartesian k-space sampling enabled the shortening of TE to 10 ms, while all the abdominal body parts were covered in a single scan including the heart, liver, kidneys, spine and spleen (Odoj *et al* 2001). Yet, relatively long TE (>5 ms) caused further signal suppression from tissue with a fast decaying ^{23}Na-signal, i.e. tissue in non-liquid environments such as cerebral tissue and cartilage. Thus, in order to acquire ^{23}Na-signal from such tissue, sequences with TE<1 ms must be used for whole body ^{23}Na investigations.

The aim of the work presented herein was to test and integrate a ^{23}Na whole body resonator on a clinical 3T system and to demonstrate that whole body ^{23}Na-MR images can be acquired with sufficiently high spatial and temporal resolution.

2. Methodology

2.1. Whole body ^{23}Na-resonator

Although the foremost design criterion for the whole body resonator system was to generate a nearly-optimal homogeneous ^{23}Na B_1-field, it was also important to cover the available volume of homogeneous B_0-field of the 3T MR system, fitting it snugly into the bore opening, leaving enough space for the patient, and to maximize its rf-transmitter efficiency, i.e. minimizing the necessary pulse length and pulse power to achieve 90° flip angle. Short rf-pulse shortens TE and thus enables the acquisition of short T_2^*-signal components.

An asymmetric 16-rung birdcage resonator (STARK Contrast, Erlangen, Germany) was designed to generate a circularly polarized B_1-field at the ^{23}Na Larmor frequency (32.6 MHz) of a 3T MRI system (Magnetom Tim Trio, Siemens Healthcare Sector, Erlangen, Germany). The asymmetric birdcage design has been previously suggested and described for X-nuclei human MRI (De Zanche *et al* 2008), when the spatial restrictions are the bore diameter plus the patient bed.

Due to the required geometric asymmetry, the capacitors on each leg had to be varied in order to maintain the electronic symmetry and to guarantee that the B_1-field across the resonator's field of view remains as homogenous as possible. The starting values for the resonator capacitors were computed from equations given elsewhere (De Zanche *et al* 2008). The final values for the capacitors on the chosen low-pass birdcage structure (see the schematic diagram in figure 1) were found through empirically adjusting each trimmer capacitor in order to achieve sufficient inter-channel decoupling and B_1-field homogeneity. The whole body resonator (figure 2) was wrapped on a Plexiglas former with 50 cm length and internal diameters of 47.5 cm (horizontal axis) and 35 cm (vertical axis), sufficiently large to fit an adult male human. The birdcage structure was surrounded by an rf-shield with 5 cm separation, which was necessary to prevent rf-coupling with the nearby gradient coils. Fine-tuning and matching was achieved on-site in loaded conditions (90 kg volunteer weight) and remained fixed tuned and matched thereafter. The influence of various loads on the resonator's tune and match properties are negligible at the low 32 MHz resonance frequency. Active decoupling was incorporated into the resonator design to enable localized signal detection with single or multiple surface receiver coils.

To characterize the performance of the birdcage volume resonator, a series of tests were carried out. The local ^{23}Na B_1-field strengths were analysed with electromagnetic field simulating software FEKO (EM Software and Systems GmbH, Böblingen, Germany) in order to assess the field of view as well as the B_1-field homogeneity and the necessary transmit power for a 90° rectangular pulse of 0.5 ms length. To simulate the electromagnetic properties of human tissue, the conductivity and electric permittivity of 0.9% saline solution was assumed inside the resonator's volume. The simulation results were practically validated by MRI on a large homogeneous phantom with 335 mm width, 335 mm length and 160 mm height scanned at three different heights within the whole body resonator. The unloaded-to-loaded quality-factor ratio (Q_0/Q_l) was determined via reflection coefficient measurement (s_{11}) using a vector network analyser (ZVL3, Rhode und Schwarz, Munich, Germany). The degree of isolation between the two channels in the loaded condition was recorded with the same vector network analyser as the transmission attenuation value (s_{21}) at 32.6 MHz.

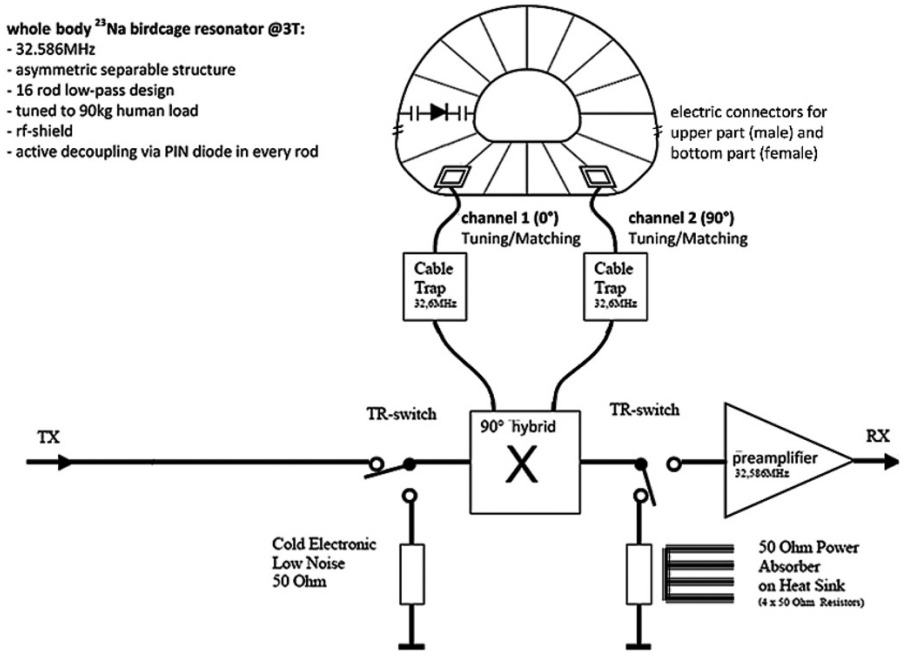

Figure 1. Schematic electronic circuit diagram for asymmetric ^{23}Na whole body birdcage resonator. Note the asymmetric feeding points in the right- and left-lower corner of the low-pass resonator. The diode shown in the figure is part of the active decoupling system. The biasing components as well as the remaining diodes and tuning capacitors in the other rungs are omitted for clarity.

2.2. RO surface resonator

A RO surface resonator was used in conjunction with the asymmetric whole body resonator TO, described above, in order to confirm the potential signal-to-noise (SNR) improvement due to localized signal detection. This dual TORO resonator system was also compared to the performance of a double-tuned ^{23}Na/^{1}H transceiver (TXRX) head resonator (quadrature birdcage with 26.5 cm inner diameter; Rapid Biomedical, Rimpar, Germany) on a bottle filled with 0.6% saline solution as well as on a healthy volunteer's head. The volunteer was positioned on the MR system bed in supine orientation for scanning with the head resonator and in prone orientation for dual resonator system operation (i.e. TO whole body resonator and RO surface resonator). The prone positioning enabled the placing of the RO surface resonator optimally on the volunteer's head with respect to the resonator sensitivity.

2.3. ^{23}Na magnetic resonance imaging

^{23}Na-MR images of phantoms and one male human volunteer were acquired with a 3D radial projection sequence with density adaption (Nagel *et al* 2009). Using this technique, a TE of 0.5 ms was achieved, which helped to minimize T_2^*-weighting effects on the measured signal intensity. The reference voltage for a 90° rectangular rf pulse of 0.5 ms length was determined via a non-localized single pulse experiment before each scan. Typical reference voltage was

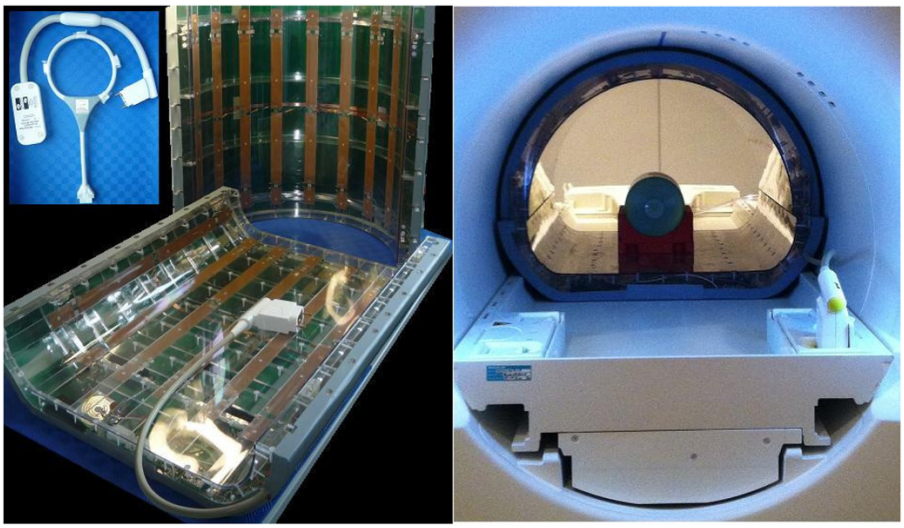

Figure 2. (Left) Split asymmetric birdcage for human whole body ^{23}Na MRI at 3T with the inset picture of ^{23}Na receive-only (RO) surface loop and adapter box. (Right) Whole body ^{23}Na-resonator together with bottle phantom placed inside the magnet bore.

measured to be 1200 V. The following sequence parameters were chosen for ^{23}Na MRI: $(6 \times 6 \times 6)$ mm^3 nominal voxel resolution, TR/TE = 49/0.5 ms, 1 ms rectangular pulse length, 60° flip angle, 10 min acquisition time and 60 Hz/pixel bandwidth. The entire body of a male human volunteer was scanned in five segments: head and shoulder, upper abdomen, lower abdomen, knees and thigh, calves and feet. The 3D datasets were reconstructed using a Kaiser–Bessel re-gridding algorithm implemented in Matlab® (The Mathworks, Natick, MA, USA) using code developed in-house. The SNR maps were computed as

$$\mathrm{SNR}_j = \frac{S_j - \overline{N_S}}{\sigma(N_S)},$$

where S_j is the signal measured in voxel j, $\overline{N_S}$ is the mean signal measured in the region of interest (RoI) representing noise chosen as a square region with 1000 pixels from a slice containing no sample tissue, and $\sigma(N_S)$ is the respective standard deviation of the noise mean. After co-registering all five data blocks qualitative whole body ^{23}Na images were generated via the sum-of-squares method.

3. Results

The unloaded-to-loaded Q-factor ratio was measured as 2.3. A decoupling of 28.5 dB was achieved between the two quadrature channels—a value typically confirming adequate isolation between channels. The B_1-field homogeneity across 66% of the inner resonator volume was better than $\pm 10\%$ as determined from simulations (figure 3). A homogeneous phantom with 335 mm length, 335 mm width, and 160 mm height filled with 0.9% saline solution was scanned in three different height positions in order to cover a similar coil volume of $(335 \times 335 \times 27)$ mm^3 (figure 4). Excellent signal homogeneity was indicated by a

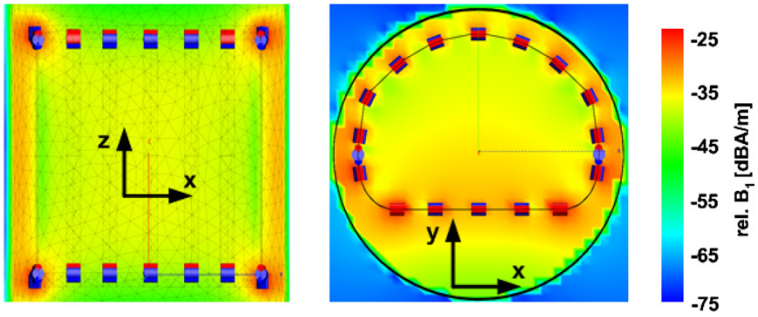

Figure 3. Simulated B_1-field for whole body ^{23}Na-resonator in coronal (left) and axial (right) views.

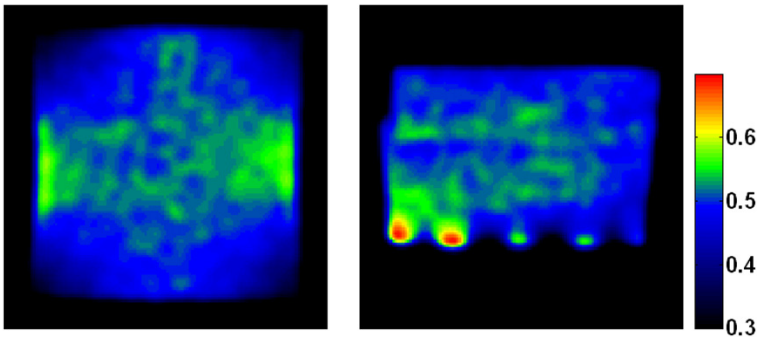

Figure 4. Coronal (left) and axial (right) ^{23}Na images of a phantom with 335 mm width, 335 mm length and 160 mm height scanned at three different heights within the whole body resonator. The phantom was filled with 0.9% NaCl saline solution. A standard deviation of 14% was measured for the mean signal inside the volume covered by the phantom. The colourbar indicates ^{23}Na-signal intensity in linearly scaled arbitrary units. Note the high ^{23}Na intensity measured at the bottom of the phantom (right) due to the close proximity of those regions to the whole body resonator's rungs.

standard deviation of 14% from the mean signal measured within the covered resonator volume. Since the B_1-field is affecting both transmit and receive sensitivities of the coil (Wetterling *et al* 2010, Alecci *et al* 2001), the B_1-field homogeneity can be assumed to be better than 7% within the volume covered by the saline phantom. Regarding the circular polarization, the presented simulations revealed that the rotating transverse magnetization generated by the birdcage varied by approximately $\pm$ 10%. Volumetric structures of (10 $\times$ 10 $\times$ 10) mm^3 and larger were resolvable as demonstrated in measurements of a standard resolution phantom; the MR images are shown in figure 5. The large field of view of the whole body resonator resulted in a large observable sample volume of approximately (45 $\times$ 45 $\times$ 35) cm^3, as determined from single segment human scans. The SNR maps of the five single segments acquired from a male volunteer were computed and are presented in axial, coronal and sagittal views in figure 6. Short TE enabled the acquisition of ^{23}Na-signal components from knee cartilage and the spinal discs. The respective SNR values are listed in table 1. Two qualitative whole body ^{23}Na images are shown in figure 7. The entire collection of sagittal and coronal whole body

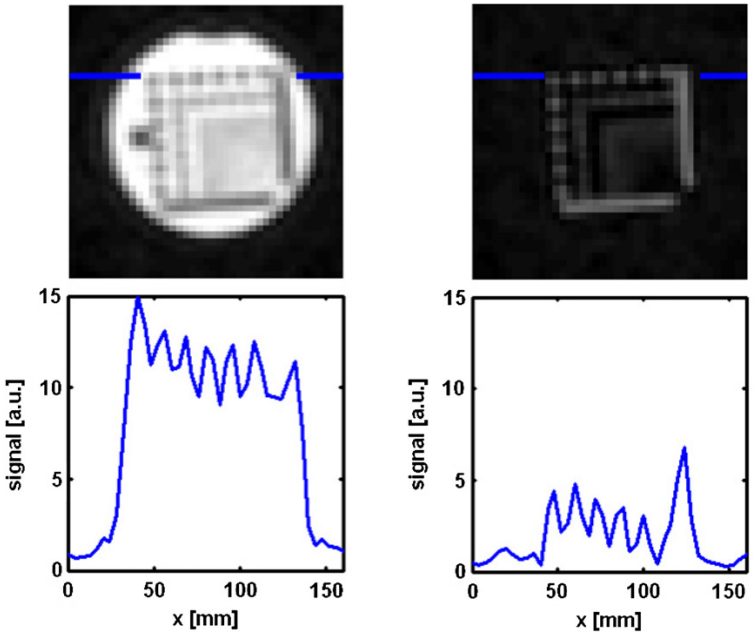

Figure 5. (Upper row) ^{23}Na-images acquired with whole body resonator of a resolution phantom with cavities immersed in (first column) and rods filled with saline solution (second column)—featuring cylindrical structures with diameters ranging from 2 to 10 mm. (Lower row) Respective profile lines through the 10 mm diameter cavities and rods plotted as a function of distance. The position of the profile lines is indicated in both images by a blue line. Structures with 10 mm diameter could be well resolved with used sequence parameters.

^{23}Na images of the male volunteer are provided in the online supplementary movie available at stacks.iop.org/PMB/57/4555/mmedia.

Comparing the performance of the double-tuned ^{23}Na/^{1}H transceiver (TXRX) head resonator with the dual resonator system (i.e. TO whole body resonator and RO surface resonator) on a phantom and the human head (figure 8) demonstrated several advantages of the dual resonator system over the conventional TXRX head resonator approach. The SNR within a volume of 10 cm of the RO surface resonator, covering the entire brain, was approximately 50% better when compared to the SNR measured in the same RoI in images acquired with the TXRX head resonator. The RO surface resonator achieved an average SNR of 75 in brain tissue, while the SNR in the same tissue was measured five times lower, i.e. 15, when measured exclusively with the whole body resonator in the TXRX mode. On the other hand, the penetration depth, which is the depth at which the ^{23}Na-signal dropped by 50% compared to the signal measured at the centre of the surface resonator, was much better for the head resonator and resulted in coverage of the entire human head including parts of the neck. The reference voltage for the head resonator was 185 V compared to 1200 V for the whole body resonator. According to the NMR theory, 12 μT B_1-field strength is required to achieve 90° flip angle with 0.5 ms rectangular pulse for ^{23}Na nuclei at 3 T. B_1-field strength of 8 nT was measured from B_1-map simulations for the whole body resonator, when 1 V was applied to its terminals. Hence, the expected reference voltage was 1500 V, well above the practically measured reference voltage of 1200 V using MRI.

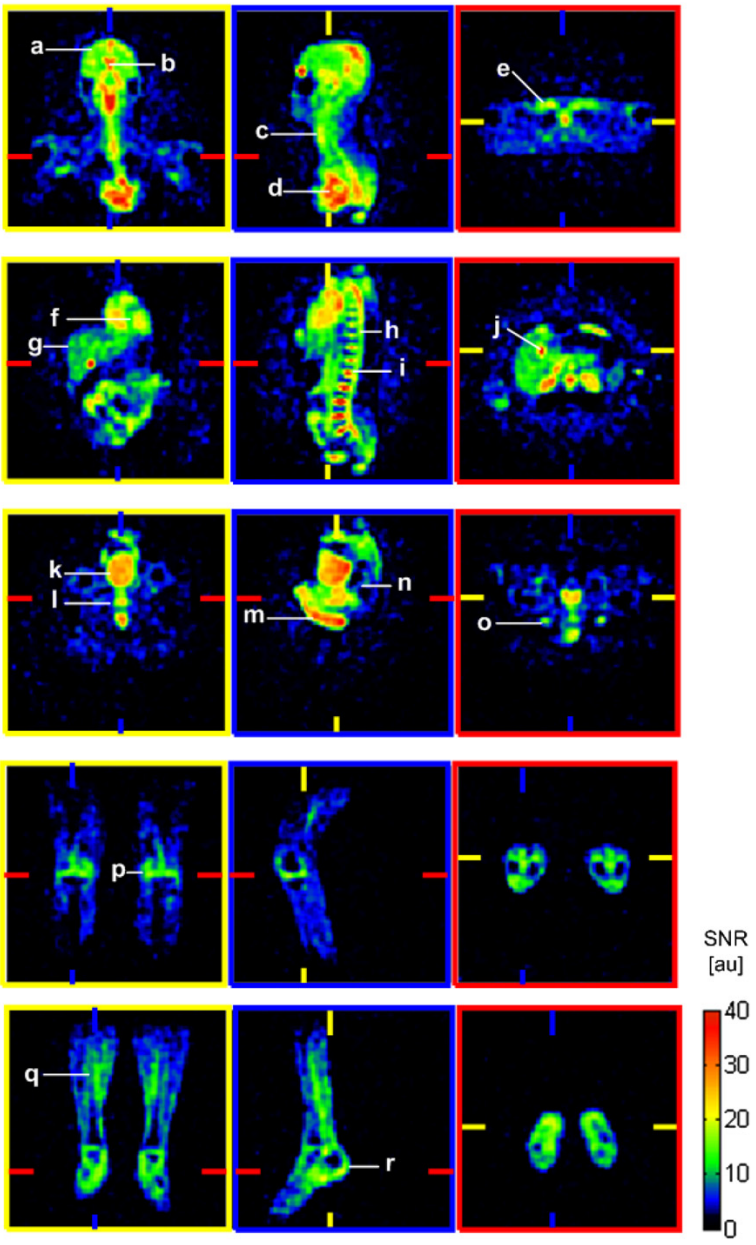

Figure 6. The SNR maps in coronal (first column, yellow frame), sagittal (second column, blue frame) and axial (third column, red frame) views for each of the five scanned segments. Colour-coded markers on the right, left, bottom and top of each map correspond to the respective orthogonal slice positions. Various structures were resolved and are marked as follows: (a) brain tissue, (b) cerebral spinal fluid, (c) thyroid, (d) ventricular blood, (e) bone marrow within the chest bone, (f) cardiac tissue, (g) liver tissue, (h) spine, (i) spinal disc, (j) gall bladder, (k) bladder, (l) prostate, (m) penis, (n) rectum (o) arterial blood, (p) knee cartilage, (q) calf tissue and (r) feet.

Table 1. Measured SNR values in different regions-of-interest (RoIs) of one male human volunteer. Data are presented as mean ± standard deviation across all voxels in one RoI.

Segment	RoI	SNR
1	Brain tissue	15 ± 2
	CSF	28 ± 3
	Eyeball	36 ± 6
	Thyroid	20 ± 2
	Blood in ventricle	32 ± 2
2	Chest bone	19 ± 2
	Myocardial tissue	11 ± 2
	Liver	11 ± 2
	Spinal channel	18 ± 5
	Vertebral disc	42 ± 5
	Gallbladder	32 ± 1
	Kidney	26 ± 1
3	Bladder	26 ± 1
	Prostate	23 ± 2
	Penis	28 ± 4
	Artery	15 ± 2
4	Knee (cartilage)	14 ± 3
5	Calf muscle tissue	9 ± 2

4. Discussion

The SNR deficit inherent to all X-nuclei MR images must be tackled not only through the use of high-field MRI systems, but also with dedicated rf-resonator systems capable of delivering sufficient SNR to produce high spatial resolution images in reasonable acquisition times. The experimental stability, which is a particularly important feature in diagnostic imaging, especially benefits from the use of homogeneous B_1-field producing a uniform flip-angle distribution across the sample. Usually, ^{23}Na MRI was focused on single regions of the human body, for instance, the brain, the heart or the knees. For this purpose, locally positioned birdcage or surface resonators are commonly used. Images presented herein, acquired with large whole body resonator, suffered from a low SNR compared to the dual resonator system (i.e. TO whole body resonator and RO surface resonator). Moreover, the restricted space inside the bore (60 cm inner diameter) and above the patient bed (∼40 cm) as well as the close proximity of the ^{23}Na whole body resonator to the ^{1}H whole body resonator and gradient system imposed a major difficulty in designing such a resonator. In order to use up the entire available space inside the bore, while maintaining an as homogeneous as possible B_1-field, an asymmetric birdcage design was chosen, as this structure had proven successful for other X-nuclei imaging studies (Purea *et al* 2010, De Zanche *et al* 2008). The inner diameter of the resonator could further be enlarged by omitting the rf-shield, using MRI scanners with larger bore size, or integrating the resonance structure into the scanner's housing. Non-clinical high-field MRI systems, which come without ^{1}H whole body resonator, could especially benefit from a ^{23}Na whole body resonator.

The circularly polarized magnetization varied in magnitude due to the geometric asymmetry of the birdcage relative to the electric feeding points on the lower right and left sides of the birdcage structure. Although electronic symmetry was restored by adjustment of capacitor values on each birdcage leg, and the inter-channel decoupling was excellent,

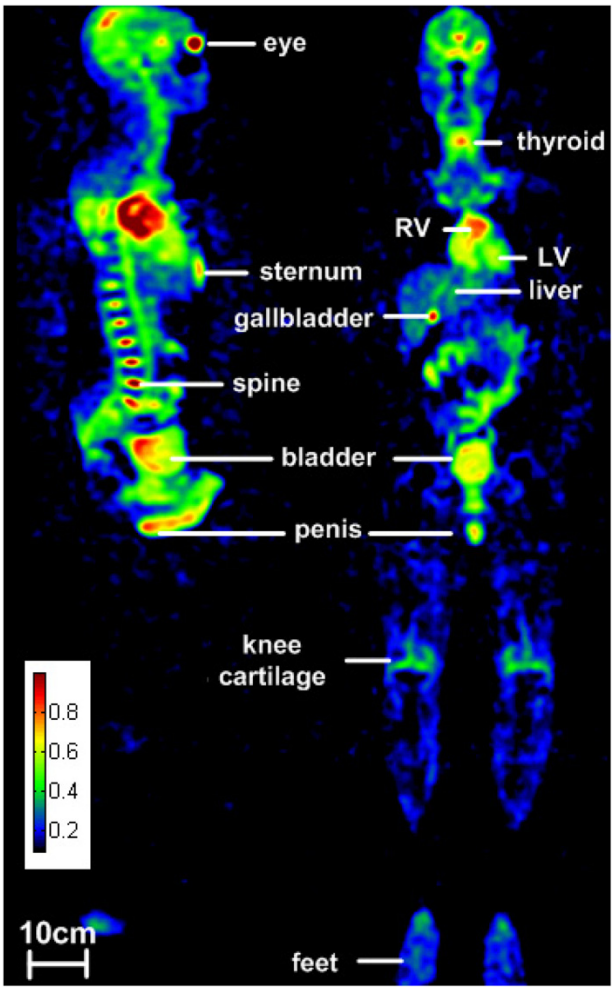

Figure 7. Qualitative ^{23}Na whole body images of a male human volunteer in sagittal and coronal views.

the magnitude variation in transverse magnetization was difficult to improve in practice. Future simulation study will focus on how to overcome this issue. Nevertheless, excellent B_1-field homogeneity was confirmed via simulations and phantom measurements. The transmit efficiency enabled the setup of 60° flip angle with 1 ms rectangular pulse. Therefore, TE was as short as 0.5 ms allowing the sampling signal from denser tissue such as cartilage. The reference voltage was six times higher, compared to a double-tuned ^{23}Na/^{1}H quadrature birdcage head resonator with 280 mm diameter and 265 mm length well in agreement with the larger dimensions of the single-tuned ^{23}Na whole body resonator. Adequately short pulse length was achieved for the Ernst angle within the legally allowed specific absorption rate levels for whole body MRI.

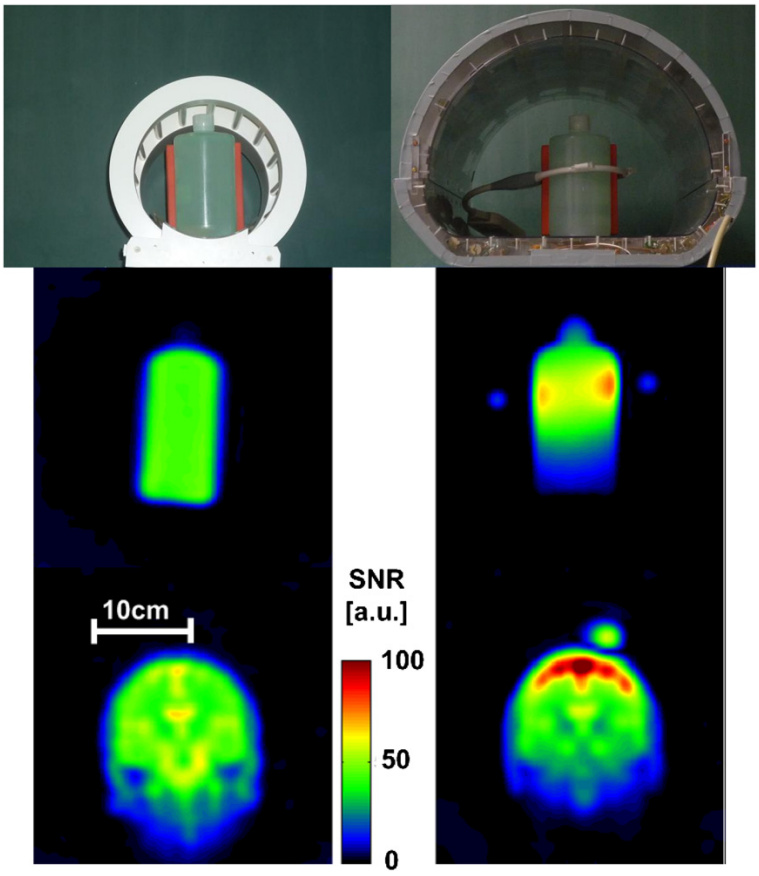

Figure 8. Comparing double-tuned $^{1}H/^{23}Na$ head resonator (left column) with single-tuned ^{23}Na dual resonator system composed of the transmit-only (TO) whole body resonator and RO surface resonator (TORO, right column). Reference vials were fixed to the loop surface resonator in order to localize its position from the TORO MR images (see dots next to bottle phantom and circle above volunteer's head). A 50% higher SNR was achieved in a spherical volume with 10 cm diameter around the surface resonator in both phantom (middle row) and brain images (lower row) compared to head coil and fivefold SNR improvement compared to TXRX whole body resonator (compare figure 6). The brain tissue SNR was measured to be ∼75 with TORO, whereas it was measured only ∼15 with TXRX whole body resonator.

It should be noted that through the circular transmit polarization and the 16-leg birdcage structure, the transmit B_1-field was made as uniform as possible with the additional benefit of increased receiver sensitivity, compared to linear resonator designs of comparable size (Odoj *et al* 2001). Compared to this earlier whole body ^{23}Na study, the better spatial resolution in the ^{23}Na images presented herein was possible due to much shorter TE, 50% higher B_0-field strength and 40% higher receive sensitivity (quadrature drive).

While the head resonator seems to be a perfect trade-off between transmit B_1-field homogeneity and receive sensitivity for a single resonator system, the dual resonator system

(i.e. TO whole body resonator and RO surface resonator) demonstrated more homogeneous B_1-field and better receive sensitivity. By arranging multiple receiver elements around the RoI, the penetration depth penalty can be overcome in the future. The fivefold SNR improvement with local receiver coil demonstrated that the combination of the whole body resonator with a local RO coil array can significantly improve the SNR in the same way as it has been reported for *in vivo* ^{23}Na surface resonators elsewhere (Wetterling *et al* 2010, 2012a, 2012b).

The SNR ratios (e.g. the blood-to-brain tissue ^{23}Na-ratio) must be considered carefully under given sequence parameters and segment acquisition protocol. For instance, T_1-weighting through short 49 ms TR and 60° flip angle as well as variations in signal sensitivity at the whole body resonator's edges hampered a direct comparison between SNR values and the TSC in different tissue types (i.e. brain, CSF and cartilage). Nevertheless, the measured SNR values can guide future studies in how to set up their ^{23}Na MRI sequence with respect to acquisition time, voxel size and resonator system. Furthermore, ^{23}Na MRI may be applied to investigate previously unconsidered body regions covering the gallbladder, intestines, penis and arms. Whole body ^{23}Na MRI may also aid in estimating tissue conductivity—an important parameter—which enables localizing bioelectrical source activity from body surface potential measurements (Wetterling *et al* 2009).

^{1}H whole body MRI has already proven useful for the assessment of cancer tissue (Meaney and Fagan 2010). Considering the close link of the TSC and tissue fate (Ouwerkerk *et al* 2007), it is expected that whole body ^{23}Na MRI can potentially aid in monitoring early response to cancer treatment. The loss of cell viability such as it occurs in cancerous and ischaemic tissue (Wetterling *et al* 2012a) could hence be determined by a strong increase in TSC long before morphological changes occur.

In conclusion, large resonator volume, relatively low rf-power consumption and high receive sensitivity in conjunction with low 0.5 ms TE enabled the acquisition of whole body ^{23}Na images with 0.2 cm^3 nominal voxel resolution in less than 60 min. Future whole body studies of the ^{23}Na-signal, as well as of the ^{23}Na relaxation parameters (i.e. T_1, and T_2^*) in tumour patients are necessary to establish whole body ^{23}Na MRI as a diagnostic monitoring technique after radio- and chemotherapy.

References

Alecci M, Collins C M, Smith M B and Jezzard P 2001 Radio frequency magnetic field mapping of a 3 Tesla birdcage coil: experimental and theoretical dependence on sample properties *Magn. Reson. Med.* **46** 379–85

Boada F E, Christensen J D, Gillen J S and Thulborn K R 1997a Three-dimensional projection imaging with half the number of projections *Magn. Reson. Med.* **37** 470–7

Boada F E, Gillen J S, Shen G X, Chang S Y and Thulborn K R 1997b Fast three-dimensional sodium imaging *Magn. Reson. Med.* **37** 706–15

Boada F E, Shen G X, Chang S Y and Thulborn K R 1997c Spectrally weighted twisted projection imaging: reducing T2 signal attenuation effects in fast three-dimensional sodium imaging *Magn. Reson. Med.* **38** 1022–8

De Zanche N, Chhina N, Teh K, Randell C, Pruessmann K P and Wild J M 2008 Asymmetric quadrature split birdcage coil for hyperpolarized 3He lung MRI at 1.5T *Magn. Reson. Med.* **60** 431–8

Hilal S K, Maudsley A A, Ra J B, Simon H E, Roschmann P, Wittekork S, Cho Z H and Mun S K 1985 *In vivo* NMR imaging of sodium-23 in the human head *J. Comput. Assist. Tomogr.* **9** 1–7

Insko E K, Clayton D B and Elliott M A 2002 *In vivo* sodium MR imaging of the intervertebral disk at 4 T *Acad. Radiol.* **9** 800–4

Jerecic R, Bock M, Nielles-Vallespin S, Wacker C, Bauer W and Schad L R 2004 ECG-gated Na-23-MRI of the human heart using a 3D-radial projection technique with ultra-short echo times *Magn. Reson. Mater. Phys. Biol. Med.* **16** 297–302

Konstandin S, Nagel A M, Heiler P M and Schad L R 2011 Two-dimensional radial acquisition technique with density adaption in sodium MRI *Magn. Reson. Med.* **65** 1091–7

Maril N, Rosen Y, Reynolds G H, Ivanishev A, Ngo L and Lenkinski R E 2006 Sodium MRI of the human kidney at 3 tesla *Magn. Reson. Med.* **56** 1229–34

Meaney J F M and Fagan A 2010 Whole-body MR imaging in a multimodality world: current applications, limitations, and future potential for comprehensive musculoskeletal imaging *Semin. Musculoskeletal Radiol.* **14** 14–21

Nagel A M, Laun F B, Weber M A, Matthies C, Semmler W and Schad L R 2009 Sodium MRI using a density-adapted 3D radial acquisition technique *Magn. Reson. Med.* **62** 1565–73

Nielles-Vallespin S, Weber M A, Bock M, Bongers A, Speier P, Combs S E, Wohrle J, Lehmann-Horn F, Essig M and Schad L R 2007 3D radial projection technique with ultrashort echo times for sodium MRI: clinical applications in human brain and skeletal muscle *Magn. Reson. Med.* **57** 74–81

Odoj F, Weisser A and Haase A 2001 Elliptical ^{23}Na body resonator *Proc. Intl. Soc. Mag. Reson. Med.* **9** 1102

Ouwerkerk R, Jacobs M A, Macura K J, Wolff A C, Stearns V, Mezban S D, Khouri N F, Bluemke D A and Bottomley P A 2007 Elevated tissue sodium concentration in malignant breast lesions detected with non-invasive ^{23}Na MRI *Breast Cancer Res. Treat.* **106** 151–60

Parish T B, Fieno D S, Fitzgerald S W and Judd R M 1997 Theoretical basis for sodium and potassium MRI of the human heart at 1.5 T *Magn. Res. Med.* **38** 653–61

Purea A, Teh K, Barlow M, Berthel D, Weisser A, Hall I and Morris P 2010 A dedicated coil configuration for hyperpolarized ^{129}Xe imaging at 1.5 T *Proc. ISMRM (Hawaii)* p 4600

Ra J B, Hilal S K, Oh C H and Mun I K 1988 *In vivo* magnetic-resonance imaging of sodium in the human-body *Magn. Reson. Med.* **7** 11–22

Schepkin V D, Ross B D, Chenevert T L, Rehemtulla A, Sharma S, Kumar M and Stojanovska J 2005 Sodium magnetic resonance imaging of chemotherapeutic response in a rat glioma *Magn. Reson. Med.* **53** 85–92

Shapiro E M, Borthakur A, Dandora R, Kriss A, Leigh J S and Reddy R 2000 Sodium visibility and quantitation in intact bovine articular cartilage using high field ^{23}Na MRI and MRS *J. Magn. Reson.* **142** 24–31

Staroswiecki E, Bangerter N K, Gurney P T, Grafendorfer T, Gold G E and Hargreaves B A 2010 *In vivo* sodium imaging of human patellar cartilage with a 3D cones sequence at 3 T and 7 T *J. Magn. Reson. Imaging* **32** 446–51

Steidle G, Graf H and Schick F 2004 Sodium 3D MRI of the human torso using a volume coil *Magn. Reson. Imaging* **22** 171–80

Thulborn K R, Davis D, Adams H, Gindin T and Zhou J 1999a Quantitative tissue sodium concentration mapping of the growth of focal cerebral tumors with sodium magnetic resonance imaging *Magn. Reson. Med.* **41** 351–9

Thulborn K R, Gindin T S, Davis D and Erb P 1999b Comprehensive MR imaging protocol for stroke management: tissue sodium concentration as a measure of tissue viability in nonhuman primate studies and in clinical studies *Radiology* **213** 156–66

Wetterling F, Gallagher L, Macrae I M, Junge S and Fagan A J 2012a Regional and temporal variations in tissue sodium concentration during the acute stroke phase *Magn. Reson. Med.* **67** 740–9

Wetterling F, Högler M, Molkenthin U, Junge S, Gallagher L, Mhairi Macrae I and Fagan A J 2012b The design of a double-tuned two-port surface resonator and its application to *in vivo* hydrogen- and sodium-MRI *J. Magn. Reson.* **217** 10–8

Wetterling F, Liehr M, Schimpf P, Liu H and Haueisen J 2009 The localization of focal heart activity via body surface potential measurements: tests in a heterogeneous torso phantom *Phys. Med. Biol.* **54** 5395–409

Wetterling F, Tabbert M, Junge S, Gallagher L, Macrae I M and Fagan A J 2010 A double-tuned H-1/Na-23 dual resonator system for tissue sodium concentration measurements in the rat brain via Na-MRI *Phys. Med. Biol.* **55** 7681–95